RSC Advances

PAPER

View Article Online
View Journal | View Issue



Cite this: *RSC Adv.*, 2021, **11**, 25477

# Design of ferrocenylseleno-dopamine derivatives to optimize the Fenton-like reaction efficiency and antitumor efficacy†

Qianya Cheng,[a] Tong Zhou,[a] Qing Xia,[a] Xiulian Lu,[a] Heng Xu,[b] Ming Hu[a] and Su Jing *[a]

Received 6th May 2021
Accepted 14th July 2021

DOI: 10.1039/d1ra03537a

rsc.li/rsc-advances

In the current study, six ferrocenylseleno-dopamine derivatives with different structural parameters were designed. Among these derivatives, **F4b**, containing two ferrocene units and a tertiary amine, showed *in vitro* anticancer activity with $IC_{50} = 2.4 \pm 0.4$ μM for MGC-803 cells, and its *in vivo* studies suggested effective antitumor activity in mice bearing an MGC-803 tumor xenograft. Mechanistic study revealed that the cytotoxicity of these ferrocenylseleno-dopamine derivatives is mainly related to the Fenton-like reaction under physiological conditions, and the tertiary amine in **F4b** can facilitate the $H_2O_2$ decomposition to generate toxic $^{\bullet}OH$ which induces apoptosis through CDK-2 inactivation.



## Introduction

The intracellular conditions of cancer cells are substantially different from those of normal ones, such as with over-expressed hydrogen peroxide, glutathione *etc.*[1,2] Designing prodrugs that respond to these internal chemicals can lead to candidates of anticancer drugs that are active against a broad range of cancers. In this endeavor, ferrocene derivatives have been developed to be a very promising field of anticancer drug candidates since ferrocerone was approved as the first ferrocenyl drug for medical use in the 1970s.[3,4] The antitumoral activities of the ferrocene unit are activated mainly by hydrogen peroxide in cancer cells. Through the Fenton-like reaction, reactive oxygen species ($^{\bullet}OH$ *etc.*) can be generated and lead to oxidative DNA damage. Various functional units, such as organic drugs, metal complexes and amino acids, have been explored in the conjugation with ferrocene to improve antitumor activity, biocompatibility, and drug transport capacity.[5–10] Up to now, the ferrocifen family developed mainly by Jaouen's group is one of the real breakthroughs in modern medicinal organometallic chemistry as anticancer drug candidates.[5–7,9]

Inspired by the promising biological activity of ferrocenyl selenoethers,[11–13] our group has previously reported a series of ferrocenylseleno-dopamine derivatives with dopamine units on the backbone, **F1a**, **F1b**, **F2a** and **F3a** listed in Table 1. These compounds were found to induce carcinoma cell apoptosis and inhibit angiogenesis of vessels in hepatocellular carcinoma.[12] It was found that the chain property between the ferrocene part and the catechol group played an important role in the anticancer properties, for example, the semi-rigidity and the rich π-electron of the benzene ring in **F1b** display a potent performance of anticancer activity. With the target to optimize antitumor efficacy, in the current study, six new derivatives listed in Table 1 were designed to fine-tune structural parameters such as spacer chain length (**F1c**, **F1d**), semi-rigidity (**F2b**), tertiary amine (**F3b** and **F4b**), or more ferrocene units (**F4a** and **F4b**). The structure–activity relationship of **F1–F4** was then explored *via* electrochemistry and Fenton-like reaction efficiency to understand the cytotoxic properties against cancer cells. Due to the importance of cyclin-dependent kinase inhibitor (CDK) in promoting transitions through the cell cycle,[14–18] the mechanistic study regarding the role of CDK2 was also investigated.

## Results and discussion

### Synthesis

The six new derivatives, **F1c**, **F1d**, **F2b**, **F3b**, **F4a** and **F4b**, were synthesized following the reported methods as shown in Scheme S1,†[12] and the detailed synthetic processes and related characterization data are provided in the ESI.† Spectroscopic studies were carried out and confirmed the structure of the as-prepared compounds (Fig. S1–S17†).

### *In vitro* anticancer activities and structure–activity relationship

The growth inhibitory effects of **F1–F4** were evaluated on human cancerous cell lines (AGS, A2780, HepG2 and MGC-803)

[a]*School of Chemistry and Molecular Engineering, Nanjing Tech University, Nanjing 211816, China. E-mail: sjing@njtech.edu.cn*

[b]*Jiangsu Province Institute of Materia Medica, Nanjing Tech University, Nanjing 211816, China*

† Electronic supplementary information (ESI) available: Cyclic voltammograms, $^1H$ NMR and HRMS spectra for compounds **F1c**, **F1d**, **F2b**, **F3b**, **F4a** and **F4b**. The growth inhibitory effect of **F4b** to normal cell line, human proximal tubular cell line (HK2). $H_2O_2$ concentration in different cell lines and migration of MGC-803 cells in the presence of **F4b**. See DOI: 10.1039/d1ra03537a

Table 1 Ferrocenyl-dopamine derivatives F1–F4

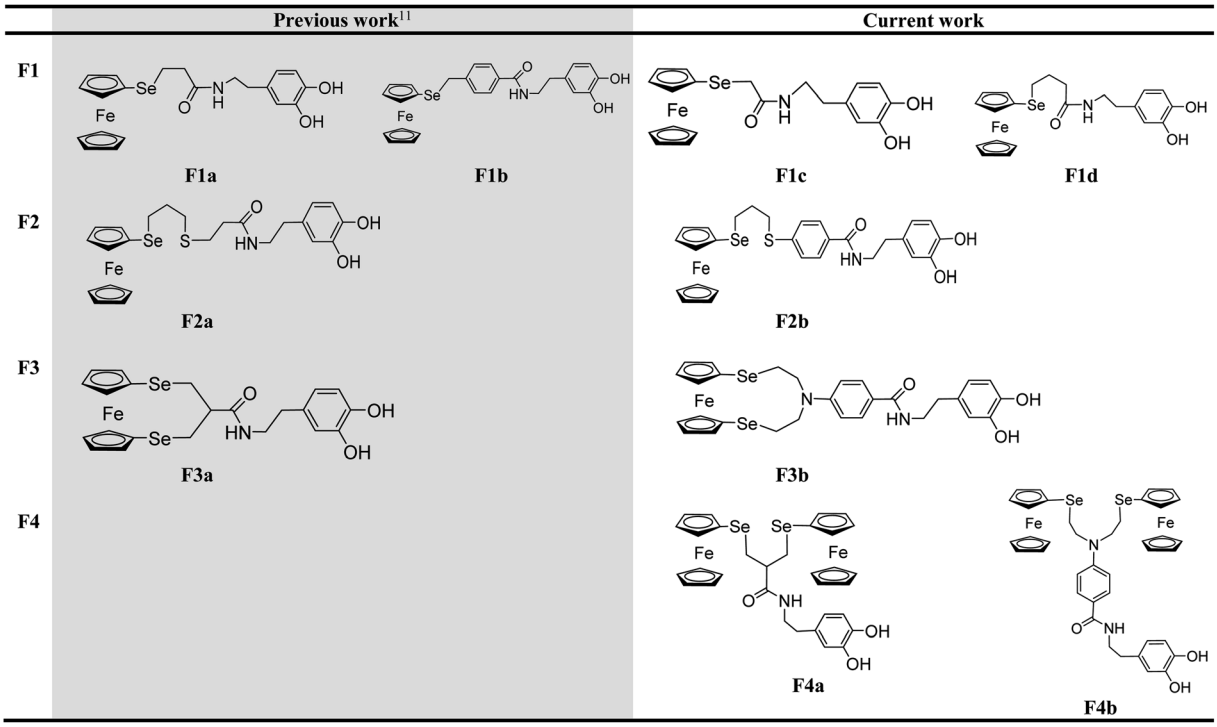


by Cell Counting Kit CCK-8 Assay. The $IC_{50}$ values of the tested compounds against cancer cells are summarized in Table 2. The results indicated that the four cell lines were all sensitive to the compounds containing two ferrocene units (**F4a** and **F4b)**, with $IC_{50}$ value below 15 μM (Fig. 1).

To understand the structure–activity relationship, the Fenton-like reaction efficiency regarding the redox properties of ferrocene unit was studied. Firstly, the redox behaviour of **F1–F4** was investigated by cyclic voltammetry (CV), the half wave potentials $E_{\frac{1}{2}}$ for oxidation of the ferrocene moiety were summarized in Table 2. The cyclic voltammograms of **F1–F4** showed one quasi-reversible redox wave in the potential range −0.5 to +1.0 V (Fig. S18–S23†), which was assigned to oxidation of the ferrocene moiety.[19] In the series **F1–F3** with only one ferrocene group, the ferrocene group in **F1d** is easier to be oxidized than that in **F1a** and **F1c**, which may be due to the long alkyl chain between the ferrocene part and the catechol group; the incorporation of phenyl group leads to higher redox

Table 2 Anticancer activity, cyclic voltammetric data and ROS generation efficacy of compounds F1–F4

| | $IC_{50}$[a] (μM) | | | | | |
|---|---|---|---|---|---|---|
| | A2780 | AGS | HepG2 | MGC-803 | $E_{\frac{1}{2}}$ ($\lvert E_{pa} - E_{pc}\rvert$)[b] (mV) | Efficacy of ˙OH generation[c] (%) |
| **F1a** | 18.5 ± 2.6 | 12.1 ± 0.6 | 14.4 ± 1.8 | 24.8 ± 4.9 | 53 (75) | 65 |
| **F1b** | 8.4 ± 0.7 | 3.7 ± 0.1 | 5.2 ± 0.8 | 12.7 ± 1.0 | 59 (72) | 61 |
| **F1c** | >50 | 42.6 ± 0.8 | 41.4 ± 0.4 | 34.8 ± 1.2 | 83 (47) | 63 |
| **F1d** | >50 | 43.1 ± 0.8 | 40.9 ± 0.1 | 30.4 ± 0.2 | 50 (65) | 60 |
| **F2a** | 12.5 ± 0.3 | 12.8 ± 2.3 | 10.6 ± 1.2 | 14.0 ± 0.9 | 49 (78) | 73 |
| **F2b** | 39.5 ± 0.5 | 9.0 ± 3.1 | >50 | 7.4 ± 1.2 | 52 (61) | 71 |
| **F3a** | 2.3 ± 0.3 | 2.4 ± 0.4 | 2.2 ± 0.5 | 4.5 ± 0.1 | −12 (54) | 80 |
| **F3b** | 21.1 ± 0.7 | 13.2 ± 0.9 | 11.7 ± 0.6 | 7.8 ± 0.9 | 13 (66) | 70 |
| **F4a** | 6.7 ± 2.2 | 6.1 ± 1.8 | 7.5 ± 1.4 | 5.6 ± 0.8 | 58 (96) | 75 |
| **F4b** | 13.5 ± 1.7 | 6.4 ± 0.5 | 7.9 ± 0.7 | 2.4 ± 0.4 | 7 (17) | 84 |
| DA | >100.0 | >50.0 | >50.0 | 28.8 ± 6.1 | 212 (594) | 29 |

[a] $IC_{50}$ measured against cancer cell lines after 72 h of treatment. $IC_{50}$ = compound concentration required to inhibit tumor cell proliferation by 50%. Data are presented as the mean ± SD from the dose–response curves at least three independent experiments. [b] $E_{\frac{1}{2}}$ values are quoted relative to $FcH/[FcH]^+$, $E_{pa}$ is the oxidation peak potential, $E_{pc}$ is the reduction peak potential. [c] The efficacy of ˙OH generation was determined using the following formula: efficacy = $(A_{665\ nm}(prodrug) - A_{665\ nm}(0))/(A_{665\ nm}(FeSO_4) - A_{665\ nm}(0))$, where $A_{665\ nm}(prodrug)$ is the absorbance of the methylene blue mixture treated with a prodrug for 2 h, $A_{665\ nm}(FeSO_4)$ is the absorbance of the same mixture treated with $FeSO_4$ for 2 h, and $A_{665\ nm}(0)$ is the absorbance of a mixture containing no iron complex.

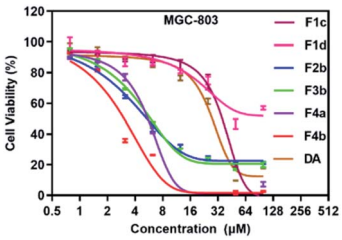


Fig. 1 Anticancer activities of F1c, F1d, F2b, F3b, F4a–b in MGC-803 cells.

potential of ferrocene, when comparing **F1d** and **F1b**, **F2a** and **F2b**; the ferrocene group in ferrocenophane **F3** is much easier to be oxidized than that of the acyclic analogues as expected. When comparing the redox property of **F3** and **F4**, the incorporation of tertiary amine leads to reverse results, **F3b** with tertiary amine showed higher $E_{\frac{1}{2}}$ than that of **F3a** (**F3a**, $E_{\frac{1}{2}} = -12$ (54) mV; **F3b**, $E_{\frac{1}{2}} = 13$ (66) mV), while **F4b** exhibited lower $E_{\frac{1}{2}}$ than **F4a** (**F4a**, $E_{\frac{1}{2}} = 58$ (96) mV; **F4b**, $E_{\frac{1}{2}} = 7$ (17) mV). This indicated the potential interaction between N and Fe in ferrocenophane **F3b** due to the structure proximity, which resulted in more positive oxidation potential of the ferrocene moiety.

It is well-established that the antitumoral activities of the ferrocene unit are activated mainly through the Fenton-like reaction with endogenous hydrogen peroxide in cancer cells to produce reactive ˙OH.[11,20,21] Therefore, the efficacy of ˙OH generation was measured to investigated the potential antitumor activity of ferrocene compound by adding **F1–F4** to a mixture of $H_2O_2$ and methylene blue (Table 2). In the studied compounds, **F1** are inefficient compared to **F2–F4** in ˙OH generation. It's expected that highest ˙OH generation efficiency can be observed from **F3a**, as its ferrocene moiety is easier to oxidize. Unexpectedly, the highest ˙OH generation efficiency was obtained from **F4b**, 86%, while its $E_{\frac{1}{2}}$ 7 (17) mV is more positive than that of **F3a** ($E_{\frac{1}{2}} = -12$ (54) mV). This is most likely caused by the tertiary amine in **F4b** which facilitates the $H_2O_2$ decomposition, same results have been obtained in the literature works.[22–25] Although **F3b** also possess the tertiary amine, it didn't show significant ˙OH generation efficiency among the tested compounds, which may be due to the interaction between N and Fe that results in more positive oxidation potential of the ferrocene moiety.

The hydrogen peroxide assay kit was performed to evaluate the intracellular $H_2O_2$ concentration of the four studied cancer cell lines. It can be found that the $H_2O_2$ concentrations in AGS and MGC-803 cells are especially overexpressed, 11.78 μM and 11.85 μM respectively (Fig. S24†). In Table 2, it can be found that the ˙OH generation efficacy of **F1–F4** is in accordance with their cytotoxicity in these two cell lines. It can be suggested that under physiological conditions, ferrocene prodrugs are activated through the Fenton-like reaction in the presence of $H_2O_2$ and generate toxic ˙OH. Among the tested compounds, **F4b** with tertiary amine group in the structure exhibited the lowest $IC_{50}$ value of 2.4 ± 0.4 μM in MGC-803 cells. Literature works have reported that the tertiary amine group can be positively charged at tumor extracellular environment through protonation, and this hydrophobic–hydrophilic transformation may enhance the internalization of **F4b** and then result in higher cytotoxicity.[26,27]

It's worth noting that **F1a**, **F1c**, and **F1d** are equally efficient in ˙OH generation, but the cytotoxicity of **F1c** and **F1d** is noticeably lower than that of **F1a**. And although replacing the ethylene (**F2a**) with phenylene (**F2b**) does not lead to significant change of ˙OH generation efficiency, the antitumor activity of **F2b** against A2780 and HepG2 cell lines is significantly reduced than that of **F2a**. These results suggest that the antitumor activity of a ferrocenylseleno-dopamine derivative correlate to but not limited to its ˙OH generation efficacy. More systematic studies are required to facilitate the in-depth understanding of this type of biologically active compound.

Among the four studied series **F1–F4**, **F4b** showed the lowest $IC_{50}$ value in MGC-803 cells. In addition, we also tested the growth inhibitory effect of **F4b** to normal cell line, human proximal tubular cell line (HK2), and found that the toxicity was almost negligible (Fig. S25†). **F4b** was then chosen to explore its biological activity using MGC-803 cells.

### Cell cycle progression and apoptosis

The cell cycle distribution of MGC-803 cells was analyzed after treatment with **F4b** (10, 20 μM) for 24 h (Fig. 2). Obvious S phase arrest can be observed in **F4b**-treated MGC-803 cells (Fig. 2a–c). As shown in Fig. 2d, cell cycle analysis indicated increased S phase proportion in comparison to that of control group. In the meantime, no significant changes in G1 phase were detected, suggesting that cell cycle S phase was arrested in response to **F4b** treatment. Meanwhile, significant decline from 12.76 to 9.39% was also observed in the $G_2$/M phase of **F4b**-treated cancer cells in comparison to that of control groups, in a dose-dependent manner.

Considering that cell cycle arrest plays an important role in apoptosis of tumor cells, the abilities of **F4b** to induce cell apoptosis or cell death in MGC-803 cells were further

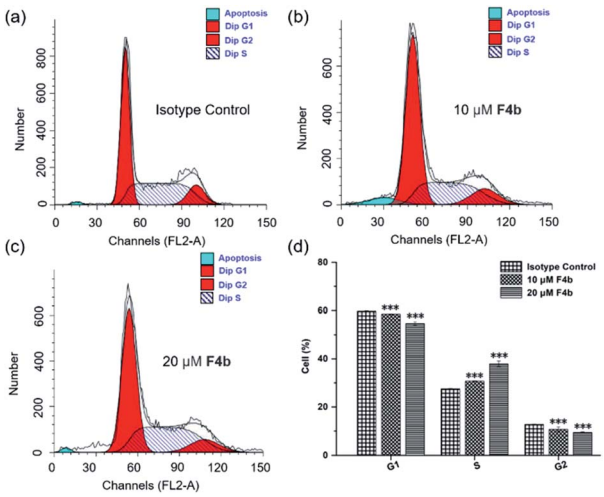


Fig. 2 Flow cytometry of cell cycle phase distribution after 24 h (a–c) and the percentage of cell cycle population (d) shown after the treatment of DA 20 μM (as an isotype control) and F4b at 10 and 20 μM. The percentage of DMSO in the medium was 1‰.

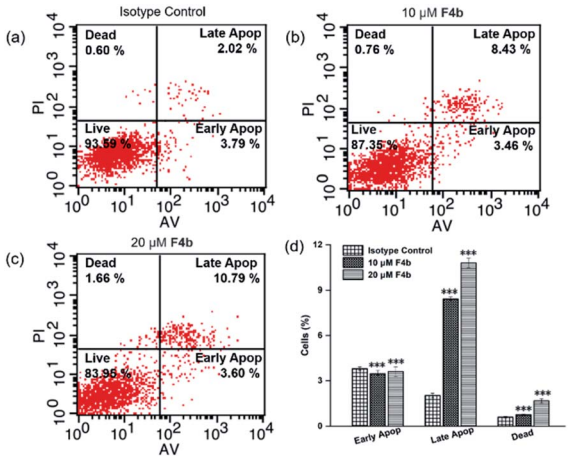


Fig. 3 F4b induces cell death in MGC-803 cells. Cells were treated with DA 20 μM (as an isotype control) and F4b at 10 and 20 μM for 24 hours. (a–c) Apoptosis was monitored by annexin V/PI double staining. (d) Percentage of early apoptotic cells, late apoptotic cells, and dead cells in MGC-803 treated with DA 20 μM and F4b at 10 and 20 μM. The percentage of DMSO in the medium was 1‰.

investigated by flow cytometry. The effects of different concentrations of **F4b** on MGC-803 cells were analyzed by annexin V/PI stain. The annexin V positive cells were regarded as apoptotic cells, including early apoptotic cells (AV+/PI−) and late apoptotic cells (AV+/PI+). As shown in Fig. 3, in comparison to the isotype control, the late apoptotic ratios of MGC-803 cells treated with 10 and 20 μM **F4b** obviously increased in a dose-dependent manner, to 8.4% and 10.8%, respectively. Moreover, the necrotic ratios of MGC-803 cells also increased in a dose-dependent manner after 10 μM and 20 μM **F4b** treatments. However, no obvious change in the early apoptotic ratios was observed in MGC-803 cells treated with 10 μM and 20 μM **F4b**. Thus, it is concluded that since the production of intracellular ˙OH, **F4b** induces MGC-803 cell apoptosis and necrosis effectively in a dose-dependent manner, resulting in directly killing cells or inhibiting cell growth.

Cell migration is an important mechanism of tumour metastasis, and the suppression of this process is a significant strategy to arrest the development of tumor.[28,29] The migration of the cell front in the presence of **F4b** (10 μM, 20 μM) was then observed at different time intervals in scratch assays performed on MGC-803 cells, the results showed that the migration of cells were effectively suppressed by **F4b** (20 μM) (Fig. S26†). These findings suggest that **F4b** inhibits the proliferation and migration of MGC-803 cells.

### Inhibition of CDK-2 expression induced by F4b

To further investigate the possible biological pathways involved in the promising antitumor effect of **F4b**, detailed mechanistic study was carried out. It is has been clearly established that cyclin-dependent kinase (CDK) inhibitor acts as a major eukaryotic protein kinase family involving in the integration of extracellular and intracellular signals to modulate gene transcription and cell division.[14–16] CDK cell cycle arrest play an important role in the apoptosis of tumor cells.[30–33] In this study, the expression of well-validated CDK-2 kinase was evaluated to examine the potential CDK cell cycle arrest. As shown in Fig. 4a–d, the results indicated that the protein level of CDK-2 was significantly decreased in a time-dependent manner after treatment with compound **F4b**. Although the relative levels of CDK2 were raising at concentration

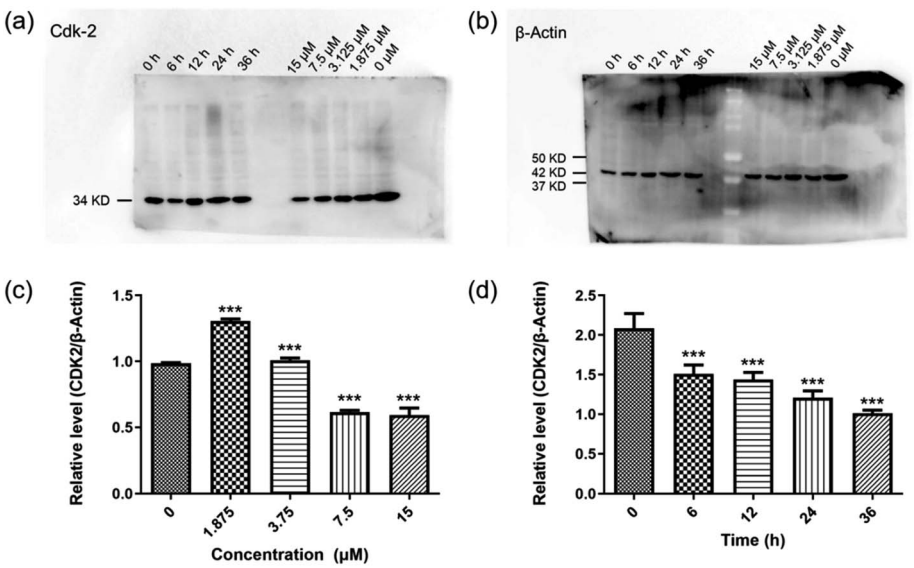


Fig. 4 Treatment of compound F4b induced S phase arrest along with a decrease of cyclin D1 in a time- and dose-dependent manner in MGC-803 cells. (a and b) Western blot analysis. The expression levels of CDK-2 and β-actin were detected after MGC-803 cells were treated with 15 μM of compound F4b for various times (0, 6, 12, 24, and 36 h) or various concentrations (0, 1.875, 3.75, 7.5, 15 μM). (c and d) The level of proteins in (a and b) was normalized to β-actin. The protein level ratios of CDK-2 in compound F4b-treated or -untreated cells (control) were depicted as histograms. Each value represents the mean ± SD of three experiments. ***, **, and * represent $p < 0.001$, $p < 0.01$, and $p < 0.05$, respectively, in comparison to control. $p < 0.05$ was considered as statistically significant.

of 1.875 μM and 3.75 μM compared to the control, the expression of CDK2 tended to decline in MGC-803 cells treated with **F4b**. It has been reported that the activation of CDK-2 triggers cell cycle transition from $G_1$ to S phase and induces DNA synthesis. In the flow cytometry study of Fig. 2, only the arrest of the cell cycle S phase was observed in response to **F4b** treatment, which can be attributed to the short $G_1$ phase.

### Evaluation of antitumor activity of F4b *in vivo*

The compound **F4b** was then performed *in vivo* antitumor evaluation in male BALB/c nude mice and MGC-803 tumor xenograft model. MGC-803 cells in PBS with matrigel/mouse were inoculated subcutaneously in the right leg flank. When the implanted tumor grew up to 50–75 $mm^3$, 24 nude mice were separated randomly into four groups (the vehicle control group, the different **F4b**-treated group, and the DA-treated group) and moved into an isotype laboratory. Mice in **F4b** treated groups were administered **F4b** (25 mg $kg^{-1}$ or 75 mg $kg^{-1}$). The control group was treated with the same concentration of DMSO. The same molar mass of DA (16 mg $kg^{-1}$) as the concentration of **F4b** (25 mg $kg^{-1}$ and 75 mg $kg^{-1}$) was used as isotype control. The body weight and the tumor volume were measured twice per week.

As shown in Fig. 5a–c, in comparison to mice in vehicle control group and the DA-treated group, the **F4b**-treated group exhibited a significant reduction in tumor volume and relative slow body weight growth (from 7.93% to 8.82%). Tumor growth inhibition rates (Fig. 5d) of the **F4b**-treated group were 72.5% (75 mg $kg^{-1}$) and 52.5% (25 mg $kg^{-1}$) respectively, while free DA showed no significant tumor inhibition effect. During the treatment, no significant loss of body weights were observed among mice in all groups (Fig. 5c), indicating the good *in vivo* bio-safety of **F4b**.

## Experimental

### Materials

The chemicals were purchased from Energy Chemical and used without further purification. Solvents were of analytical-reagent (AR) grade and were used without any further purification. Diferrocenyl diselenide, and 1,2,3-triselena ferrocenophane were prepared according to literature methods.[34] A2780, AGS, MGC-803, and HepG2 cells were grown in media supplemented with 0.5 μL $mL^{-1}$ of streptomycin (Invitrogen, USA) at 37 °C with 5% $CO_2$. Stock solutions (100 mM) of the different compounds were obtained by dissolving them DMSO.

### Methods

All manipulations involving air-free syntheses were performed using standard Schlenk-line techniques under a nitrogen atmosphere. NMR spectra were recorded at ambient temperature on a Bruker AV400 spectrometer ($^1$H NMR at 400 MHz, $^{13}$C NMR at 100.6 MHz), chemical shifts ($\delta$) are given in ppm using DMSO-$d_6$ as solvent. HRMS were recorded on a time-of-flight (TOF) mass analyzer using electrospray ionization and analyzed using the MassLynx software suite. Melting points (mp) were determined with an X-5 Microscopic melting point meter. IR spectra were recorded in the range 4000–400 $cm^{-1}$ using KBr pellets on a Bruker Vector 22 FT-IR spectrophotometer. Cyclic voltammograms were recorded using a CH Instruments 660D electrochemical analyzer (Shanghai Chenhua).

### Cytotoxicity assay

The effects of the compounds on cancer cell proliferation were performed. Cell viability was determined using cell counting

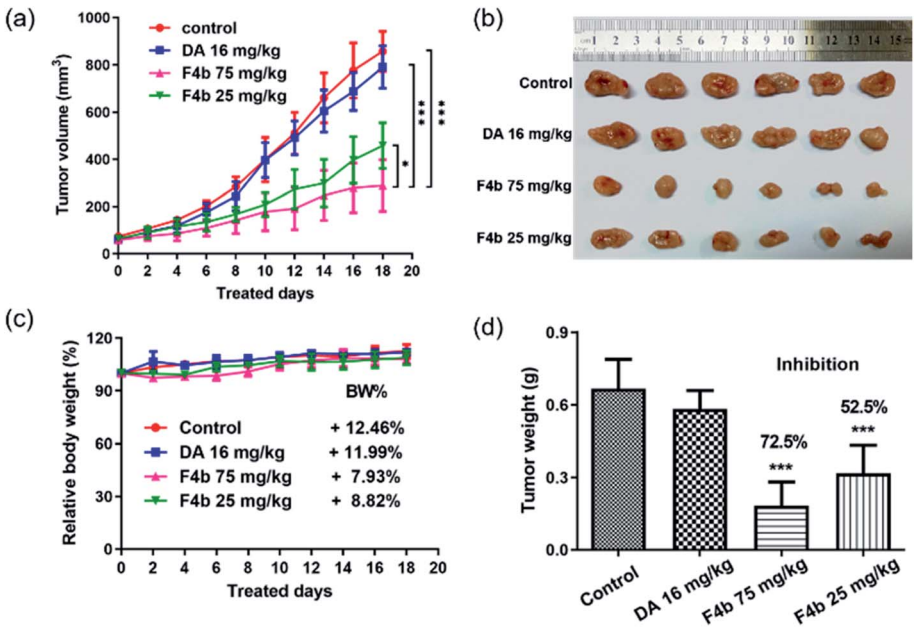


Fig. 5 *In vivo* anticancer activity of **F4b** in mice bearing MGC-803 tumor xenograft. (a) Effect of **F4b** (75, 25 mg $kg^{-1}$/p2d), DA (16 mg $kg^{-1}$/p2d), or vehicle (5% DMSO in saline, v/v) on growth of tumor xenograft. Tumor growth was tracked by the mean tumor volume ($mm^3$) ± SD ($n = 6$). (b) Photographs of tumor from the treatment groups and the control group. (c) Body weight change (presented as % change from initial weight). (d) Tumor growth inhibition rate.

kit-8 (CCK-8, Dojindo Laboratories, Japan). In brief, cancer cells were seeded into 96-well plates at a density of $4 \times 10^3$ (50 μL) per well, then incubated for 6 h at 37 °C. After incubation, according to compound concentration, the compounds were serially diluted in the medium from 200 μM, respectively. Then, 50 μL suspensions were mixed with cells at an equal volume. After incubation for 72 h at 37 °C, cells were incubated with 10 μL of CCK-8 for 3 h at 37 °C. Then, the absorbance was measured at 450 nm by use of a microplate reader (Thermo, USA). Wells with untreated cells or DMSO were used as controls. Cell survival rate curves were plotted as a percentage of untreated control cells according to standard curves, and $IC_{50}$ values were calculated. The percentage of DMSO in the medium never exceeded 1‰. This was also the maximum DMSO concentration in all cell-based assays described below.

### Cell migration assay

For the cell migration assay, MGC-803 cells were seeded in a 24-well plate and kept for 1 day. A 10 μL sterile pipette tip was used to introduce a scratch on the plate. The cells were charged with **F4b** (10 μM and 20 μM). In the control experiment, no drug was added. Still images were captured after different time intervals for 48 h to measure migration speed.

### Cell cycle analysis

Cells were cultured in the presence of different concentrations of the **F4b** (0, 10 and 20 μM) for 24 h. The same concentrations of DMSO were used as isotype control. MGC-803 cells were harvested, fixed with 75% ethanol at −20 °C overnight, and then stained with 50 μg $mL^{-1}$ propidine iodide containing 0.25 mg $mL^{-1}$ of RNase A at room temperature for 30 min. Analysis was performed by flow cytometry (Becton-Dickinson FACSCalibur).

### Cell death analysis

The extent of apoptosis was measured with an annexin V FITC/PI apoptosis detection kit (Invitrogen, CA, USA) according to the manufacturer's instructions. MGC-803 cells were treated with **F4b** (0, 10 and 20 μM) for 24 h. The same concentrations of DMSO were used as isotype control. MGC-803 cells were then washed with ice-cold PBS and incubated with a combination of 5 μL of FITC annexin V and 5 μL of PI at room temperature in the dark for 15 min. Analysis was performed by flow cytometry (BD, USA). Each determination was repeated three times.

### Western blotting

A portion of $1 \times 10^6$ MGC-803 cells was treated with **F4b** (20 μM) and collected at 0, 12, 24, 36, and 48 h after the compound incubation. After centrifugation at 500 rpm for 5 min, the pellet was lysed with P-MER cell lyse buffer (1 mL) (Thermo Scientific, USA) containing 1% Halt Protease and Phosphatase Inhibitor Cocktail (Thermo Scientific, USA) for 30 min on ice. The supernatant was collected after 10 min of centrifugation, equaled by spectrophotometer, denatured with sample loading buffer for 10 min at 95 °C, and stored at 4 °C for future use. Cell lysate proteins (50 μg per lane) were loaded on an SDS-PAGE instrument, transferred to a PVDF instrument (Bio-Rad, USA), immune-blotted with mAb AC10364 at 4 °C overnight, and probed with specific Abs as indicated, such as β-actin and CDK-2 (cell signaling).

### Monitoring generation of ROS by methylene blue

A solution (25 mL) containing PB buffer (20 μM, pH 7.0), EDTA (10 μM), methylene blue (12 μM), and 15 μM hydrogen peroxide ($H_2O_2$) at 37 °C with constant stirring. After 5 min, an iron complex (10 μM, ferrocene prodrugs) was added. After 2 h, monitoring of the absorbance of this solution. The efficacy of ROS generation was determined using the following formula: efficacy $= (A_{665\ nm}(\text{prodrug}) - A_{665\ nm}(0))/(A_{665\ nm}(FeSO_4) - A_{665\ nm}(0))$, where $A_{665\ nm}$(prodrug) is the absorbance of the methylene blue mixture treated with a prodrug for 2 h, $A_{665\ nm}(FeSO_4)$ is the absorbance of the same mixture treated with $FeSO_4$ for 2 h, and $A_{665\ nm}(0)$ is the absorbance of a mixture containing no iron complex.

### Hydrogen peroxide content

Intracellular $H_2O_2$ was determined using the hydrogen peroxide assay kit according to the manufacturer's protocol. A portion of $1 \times 10^6$ cells was collected and high-speed centrifugation at low temperature (12 000 rpm, 4 °C), 5 min. After centrifugation the original medium was discarded, cells precipitates were collected, add 100 μL peroxide hydrogen cracking fluid percussion blending, 12 000 rpm, 4 °C for 5 min, take supernatant for subsequent determination. Each test tube to join 50 μL samples and 100 μL hydrogen peroxide reagent, blending, and moved into 96-well plates, 30 min at room temperature, determine the absorbance of $A_{560}$, according to the standard curve to calculate concentration of hydrogen peroxide.

### Tumor xenograft

To study the efficacy of **F4b** as an anticancer drug, tumor-bearing nude mouse experiments were performed through a MGC-803 tumor xenograft. The nude mice of BALB/C strain (female, 19–20 g body weight) were purchased from the Vital River Laboratory Animal Technology Co., Ltd. (Beijing, China). The mice were raised at the Center for Laboratory Animals, Nanjing Medical University. All animal procedures were performed in accordance with the Guidelines for Care and Use of Laboratory Animals of Nanjing Medical University and experiments were approved by the Animal Ethics Committee of Nanjing Medical University. A portion of $2 \times 10^6$ MGC-803 cells in 100 μL of PBS with matrigel (BD Biosciences, USA) (1/1) per mouse were inoculated subcutaneously in the right leg flank. When the implanted tumor grew to 50–75 $mm^3$, 24 nude mice were separated randomly into four groups (to be described later) and moved into the isotope laboratory. The body weight and the tumor volume were measured twice per week. A group of mice was treated with **F4b** (25 mg $kg^{-1}$ and 25 mg $kg^{-1}$). The control group was treated with same concentration of DMSO. The same molar mass of DA (16 mg $kg^{-1}$) as the concentration of **F4b** (25 mg $kg^{-1}$ and 25 mg $kg^{-1}$) was used as isotype control. The compounds were managed once every 2 days for 3 weeks.

Tumor volume was measured by calipers every 2 days post-treatment and calculated as 0.5 × length × (width)$^2$. Tumors were weighed and collected after slaughter.

### Statistical analysis

All experiments were performed in triplicate; statistical analysis was performed with the aid of commercially available software (GraphPad Prism 6, GraphPad Software Inc., San Diego, CA). Results are expressed as the mean ± SD. One-way ANOVA was used to compare groups. ***, **, and * represent $p < 0.001$, $p < 0.01$, and $p < 0.05$, respectively, in comparison to control.

## Conclusions

Ferrocene derivatives have been developed to be promising candidates of anticancer drugs owing to their ability to catalyze hydrogen peroxide in cancer cells through Fenton-like reaction and generate cytotoxic reactive oxygen species. In this study, six ferrocenylseleno-dopamine derivatives were prepared to optimize the Fenton-like reaction efficiency and antitumor efficacy by fine-tuning a panel of structural parameters. Among all the candidates, **F4b** exhibited the lowest $IC_{50}$ value 2.4 ± 0.4 μM for MGC-803 cells. This is most likely caused by the tertiary amine in **F4b** which facilitates the $H_2O_2$ decomposition. In addition, mechanistic study revealed that the ferrocenylseleno-dopamine derivatives can induces apoptotic cell death through CDK-2 inactivation. Moreover, *in vivo* study confirmed effective inhibition of tumor growth with no obvious bio-safety issue suggesting the promising potential of ferrocenylseleno-dopamine derivatives in future therapeutic applications.

## Conflicts of interest

There are no conflicts to declare.

## Acknowledgements

We gratefully acknowledge financial support from the National Natural Science Foundation (Grant No. 21671101).

## Notes and references

1 L. S. Lin, J. B. Song, L. Song, K. M. Ke, Y. I. Liu, Z. J. Zhou, Z. Y. Shen, J. Li, Z. Yang, W. Tang, G. Niu, H. H. Yang and X. Y. Chen, *Angew. Chem., Int. Ed.*, 2018, **57**, 4902–4906.
2 J. Sun, K. Du, J. J. Diao, X. T. Cai, F. D. Feng and S. Wang, *Angew. Chem., Int. Ed.*, 2020, **59**, 12122–12128.
3 M. Patra and G. Gasser, *Nat. Rev. Chem.*, 2017, **1**, 1–12.
4 R. Wang, H. H. Chen, W. T. Yan, M. W. Zheng, T. S. Zhang and Y. H. Zhang, *Eur. J. Med. Chem.*, 2020, **190**, 112109.
5 G. Jaouen, A. Vessières and S. Top, *Chem. Soc. Rev.*, 2015, **44**, 8802–8817.
6 Y. Wang, P. M. Pigeon, S. Top, M. J. McGlinchey and G. Jaouen, *Angew. Chem., Int. Ed.*, 2015, **54**, 10230–10233.
7 Y. Wang, P. M. Dansette, P. Pigeon, S. Top, M. J. McGlinchey, D. Mansuy and G. Jaouen, *Chem. Sci.*, 2018, **9**, 70–78.
8 A. Singh, I. Lumb, V. Mehra and V. Kumar, *Dalton Trans.*, 2019, **48**, 2840–2860.
9 K. Kowalski, *Coord. Chem. Rev.*, 2018, **366**, 91–108.
10 K. Kowalski, *Coord. Chem. Rev.*, 2021, **432**, 213705.
11 J. M. Zhou, X. F. Zhu, Q. Y. Cheng, Y. X. Wang, R. Q. Wang, X. W. Cheng, J. J. Xu, K. T. Liu, L. Li, X. M. Li, M. F. He, J. Wang, H. Xu, S. Jing and L. Huang, *Inorg. Chem.*, 2020, **59**, 9177–9187.
12 H.-Y. Zhou, M. Li, J. Qu, S. Jing, H. Xu, J.-Z. Zhao, J. Zhang and M.-F. He, *Organometallics*, 2016, **35**, 1866–1875.
13 J. Qu, Q. Xia, W. Ji, S. Jing, D. R. Zhu, L. Li, L. Huang, Z. F. An, C. Q. Xin, Y. Ni, M. X. Li, J. D. Jia, Y. L. Song and W. Huang, *Dalton Trans.*, 2018, **47**, 1479–1487.
14 M. Malumbres and M. Barbacid, *Trends Biochem. Sci.*, 2005, **30**, 630–641.
15 S. Lim and P. Kaldis, *Development*, 2013, **140**, 3079–3093.
16 M. Malumbres and M. Barbacid, *Nat. Rev. Cancer*, 2009, **9**, 153–166.
17 P. Xia, Y. Liu, J. Chen, S. Coates, D. X. Liu and Z. K. Cheng, *J. Biol. Chem.*, 2018, **293**, 19672–19685.
18 M. Malumbres, *Genome Biol.*, 2014, **15**, 1–10.
19 W. S. Chen, W. Z. Ou, L. Q. Wang, Y. Q. Hao, J. S. Cheng, J. Li and Y. N. Liu, *Dalton Trans.*, 2013, **42**, 15678–15686.
20 C. Fang, Z. Deng, G. Cao, Q. Chu, Y. Wu, X. Li, X. Peng and G. Han, *Adv. Funct. Mater.*, 2020, **30**, 1910085.
21 Z. Tang, P. Zhao, H. Wang, Y. Liu and W. Bu, *Chem. Rev.*, 2021, **121**, 1981–2019.
22 Y. D. Du, C. W. Tse, Z. J. Xu, Y. G. Liu and C. M. Che, *Chem. Commun.*, 2014, **50**, 12669–12672.
23 M. Colladon, A. Scarso and G. Strukul, *Green Chem.*, 2008, **10**, 793–798.
24 S. I. Murahashi, T. Nakae, H. Terai and N. Komiya, *J. Am. Chem. Soc.*, 2008, **130**, 11005–11012.
25 K. Bergstad and J. E. Bäckvall, *J. Org. Chem.*, 1998, **63**, 6650–6655.
26 Q. Chen, J. W. Zheng, X. Z. Yuan, J. F. Wang and L. J. Zhang, *Mater. Sci. Eng. C*, 2018, **82**, 1–9.
27 Y. Q. Shang, N. Zheng and Z. G. Wang, *Biomacromolecules*, 2019, **20**, 4602–4610.
28 G. Bergers and L. E. Benjamin, *Nat. Rev. Cancer*, 2003, **3**, 401–410.
29 C. H. Stuelten, C. A. Parent and D. J. Montell, *Nat. Rev. Cancer*, 2018, **18**, 296–312.
30 G. H. Zhang, F. E. Ma, L. Q. Li, J. J. Li, P. P. Li, S. L. Zeng, H. B. Sun and E. G. Li, *Biochem. Pharmacol.*, 2019, **163**, 133–141.
31 P. C. Diao, W. Y. Lin, X. E. Jian, Y. H. Li, W. W. You and P. L. Zhao, *Eur. J. Med. Chem.*, 2019, **179**, 196–207.
32 P. Xia, J. R. Chen, Y. N. Liu, M. Fletcher, B. C. Jensen and Z. G. Cheng, *J. Biol. Chem.*, 2020, **295**, 4265–4276.
33 K. Hiromura, J. W. Pippin, M. J. Blonski, J. M. Roberts and S. J. Shankland, *Oncogene*, 2002, **21**, 1750–1758.
34 M. R. Burgess, S. Jing, C. P. Morley and C. Thöne, *J. Organomet. Chem.*, 2006, **691**, 4963–4967.